Title

Temperature-dependent kinetics of the reactions of CH2OO with acetone, biacetyl, and acetylacetone

Journal

International Journal of Chemical Kinetics, 55(3)

ISSN

0538-8066

Authors

Cornwell, Zachary A
Enders, Jonas J
Harrison, Aaron W
et al.

Publication Date

2023-03-01

DOI

10.1002/kin.21625

Peer reviewed

Temperature-Dependent Kinetics of the Reactions of CH_2OO with Acetone, Biacetyl, and Acetylacetone

Zachary A. Cornwell,[1] Jonas J. Enders,[1] Aaron W. Harrison,[2] and Craig Murray[*,1]

1. *Department of Chemistry, University of California, Irvine, Irvine CA 92697, USA*
2. *Department of Chemistry, Austin College, Sherman, TX 75090, USA*

[*] Email: craig.murray@uci.edu; Telephone: +1-949-824-4218

Abstract

Temperature-dependent rate constants for the reactions of CH_2OO with acetone (Ac), biacetyl (BiAc), and acetylacetone (AcAc) have been measured over the range 275–335 K using a flash photolysis, transient absorption spectroscopy technique. The measurements were performed at a total pressure of ~80 Torr in N_2 bath gas, which corresponds to the high-pressure limit for these reactions. All three reactions show linear Arrhenius plots with negative temperature dependences. Rate constants increase in the order Ac < AcAc ≪ BiAc across the temperature range; at 295 K the rate constants are k_{Ac} = (4.8±0.4)×10^{-13} cm^3 s^{-1}, k_{AcAc} = (8.0±0.7)×10^{-13} cm^3 s^{-1}, and k_{BiAc} = (1.10±0.09)×10^{-11} cm^3 s^{-1}. Sensitivity to temperature, characterized by the magnitude of the negative activation energy, increases in the order AcAc < BiAc < Ac (E_a /R values of –1830±170 K, –1260±170 K, and –460±180 K, respectively). CBS-QB3 calculations show that the Ac and BiAc reactions proceed via formation of an entrance channel complex followed by 1,3-dipolar cycloaddition to form secondary ozonide products via a submerged transition state. For the BiAc reaction, the rate limiting step appears to be rearrangement of a long-range van der Waals complex into the short-range complex that subsequently leads directly to the cycloaddition transition state with a very low energy barrier. The calculations show that two reaction pathways are competitive for AcAc with nearly identical transition state free energies ($\Delta G°$ = +10.1 kcal mol^{-1} at 298 K) found for cycloaddition at the C=O and at the C=C site of the dominant enolone tautomer. The weak temperature dependence observed is likely due to competition between these pathways.

Introduction

Gas phase alkene ozonolysis proceeds via the well-established Criegee mechanism of 1,3-cycloaddition across the olefinic bond to form a cyclic primary ozonide (POZ), which promptly decomposes into a carbonyl oxide, known as a Criegee intermediate, and a carbonyl compound.[1] In the troposphere, energized Criegee intermediates (CIs) formed in the ozonolysis of volatile organic compounds (VOCs) either undergo unimolecular decomposition, typically generating OH radicals, or are stabilized by collisions and subsequently removed by reaction with trace atmospheric gases.[2–4] Over the last decade, the development of more efficient photochemical production methods has stimulated a surge of interest in the properties and chemistry of a range of CIs.[5–11] The single most important reactive sink in the troposphere for the simplest CI (formaldehyde oxide, CH_2OO), which is a major product in the ozonolysis of isoprene and other terminal or exocyclic alkenes,[12] is water vapor, overwhelmingly in the form of water dimer.[11] Reactions with other trace species such as organic acids, SO_2, and carbonyl compounds may be important in some environments, as well as for substituted CIs.[10,11]

Carbonyl compounds are an important class of VOCs that directly influence the oxidative capacity of the atmosphere through production of O_3 and formation of secondary organic aerosols (SOAs).[13–15] CIs have been shown in ozonolysis experiments to react with aldehydes and ketones through a 1,3-dipolar cycloaddition across the carbonyl to form a cyclic 1,2,4-trioxolane secondary ozonide (SOZ).[16–20] More recent experiments have quantified the rate constants of the reactions of CH_2OO with acetone and other carbonyls.[21–26] Table 1 summarizes measurements near room temperature of the rate constant for the reaction of CH_2OO with acetone, one of the most abundant carbonyl compounds in the atmosphere.[15] The experimental measurements are in reasonably good agreement, with rate constants of $\sim 10^{-13}$ cm^3 s^{-1}. Photoionization mass spectrometry (PIMS) measurements also identified the formation of SOZ products.[21] Kinetics measurements performed across the range 250–500 K find

a marked negative temperature dependence.[23,25] Pressure-dependent measurements in N_2 bath gas find that the rate constant increases with pressure and that the high-pressure limit is reached by ~30 Torr;[25] the smaller rate constants observed in He bath gas at similar pressures[23] suggest that the identity of the bath gas affects the high-pressure limit. The temperature and pressure dependences are consistent with computational work for CI + carbonyl reactions that has suggested the reaction proceeds by the formation of an entrance-channel van der Waals (vdW) complex followed by passage over the cycloaddition transition state (TS) that leads directly to the SOZ product.[23,27–30] More

Table 1 Compiled rate constants for CH_2OO + acetone reaction at or near room temperature. Uncertainties are 1σ.

k_{Ac} / 10^{-13} cm^3 s^{-1}	T / K	P / Torr	Bath gas	Reference
2.3±0.3	293	4	He	Taatjes et al.[21]
3.0±0.6	298	25	He	Elsamra et al.[23]
3.4±0.9	297	760	air	Berndt et al.[22]
4.7±0.1	295	30–100	N_2	Chhantyal-Pun et al.[25]
4.1±0.1	295	67	N_2	Cornwell et al.[26]

recently, Wang et al. have identified longer range vdW complexes and rearrangement TSs in the reactions of CH_2OO with acetaldehyde and acetone.[31] In the case of acetaldehyde, the novel rearrangement TS that separates the outer and inner vdW complexes was found to be rate-limiting.

Rate constants for CI + aldehyde and ketone cycloaddition reactions strongly depend on the identity of the carbonyl substituents.[21,24,26,32] Acetaldehyde has a rate constant approximately three times larger than acetone,[21,23] while for hexafluoroacetone (HFA) the rate constant is two orders of magnitude larger.[21] Increased rate constants relative to acetone were also found in our previous

work on the reactions of CH_2OO with α-diketones for which rate constants were ~30 times larger than that of acetone, while β-diketones react with similar rate constants.[26] The difference in rate constants can be attributed to a stabilization of the TS, which can be understood from frontier molecular orbital theory considerations.[33–35] The presence of electron-withdrawing substituents lowers the energy of the lowest unoccupied molecular orbital (LUMO) of the carbonyl (the dipolarophile), reducing the energy mismatch with highest occupied molecular orbital (HOMO) of the CI (the 1,3-dipole). Correlations (or anti-correlations) identified between the experimental rate constants and either the orbital energy gap or compiled σ_p Hammett substituent parameters[36] may prove useful in the development of structure-activity relationships (SARs). The effect of conjugation on reactivity when unsaturated vinyl or allyl substituents are present is less clear.[24,32] PIMS measurements confirmed that the methyl vinyl ketone (MVK) and methacrolein (MACR) reactions occurred at the carbonyl rather than the alkene site, for which much slower rate constants have been measured.[37] Despite being an enone and enal respectively, rate constants for MVK and MACR are similar to that of acetone,[24] while acrolein (ACR) reacts with a rate constant similar to that of acetaldehyde.[32]

Here, we describe the results of experimental and computational work that explores the temperature-dependent kinetics of the reactions of CH_2OO with acetone (Ac), biacetyl (BiAc), and acetylacetone (AcAc), extending our previous study.[26] Ac and BiAc are prototypical ketone and α-diketone species, respectively, while AcAc exists primarily as its enolone tautomer. The reaction kinetics are studied over the temperature range of 275–335 K at a pressure of 80 Torr using laser flash photolysis transient absorption spectroscopy. Complementary *ab initio* calculations characterize stationary points on the reaction potential energy surfaces, suggesting that the loose outer TS is rate-limiting in the BiAc reaction and identifying several new reaction pathways in the AcAc reaction.

Experimental and theoretical methods

Laser flash photolysis transient absorption spectroscopy measurements of the reaction kinetics were performed in a recently upgraded apparatus. The stainless steel flow reactor used in our previous Criegee intermediate kinetics studies[26,38,39] has been replaced by a jacketed glass reactor. The total reactor length is 132 cm, with an internal diameter of 2.5 cm. The central 90 cm between the gas inlet and outlet ports are jacketed and can be temperature controlled. The cell temperature is controlled using a unistat (Huber Tango) and can be varied from 228–523 K. Two Type K thermocouples positioned at each end of the flow reactor measure the temperature; the measurements agree to within < 1 K and are stable within the same range over the course of experimental kinetics runs. The reactant gas mixture inlet and outlet are positioned within the temperature-controlled region of the apparatus (20 cm from the windows). The windows are purged with a flow of N_2 to reduce build-up of residue. The pressure inside the apparatus is measured with a capacitance manometer (MKS, 902B) situated centrally.

The flow reactor is evacuated to a base pressure of < 10 mTorr by a rotary vane pump (Leybold Oerlikon D16B), throttled by a variable flow valve. Gas flow rates into the reactor are controlled using choked flow orifices (O'Keefe), selected to achieve a total flow rate of ~3.8 sLpm. The cell is operated at a static pressure of ~80 Torr (stable to within < 1 Torr). The total gas flow comprises a mixture of CH_2I_2, O_2, N_2, and reactant X (where X = Ac, BiAc, or AcAc). Gases O_2 (Airgas, UHP 4.4) and N_2 (Airgas, HP 4.8) are used directly from the cylinders. Liquids are placed in smog bubblers (Ace Glass) and carried into the reactor by a flow of N_2. The smog bubblers are maintained at either 273 K in a water/ice slush or 295 K in a temperature-controlled water bath to ensure stability of the liquid vapor pressure. Concentrations are estimated based on the fractional contributions to the total flow and the mole fraction present. Typically, we use $[CH_2I_2] = 1\times10^{15}$ cm^{-3}, $[O_2] = 2.1\times10^{17}$ cm^{-3}, $[X] \leq 2.4\times10^{16}$ cm^{-3}, with N_2 balance. Calibration measurements, in which the carbonyl spectrum is

recorded using LEDs centered at 280 nm (Ac, AcAc) or 420 nm (BiAc) using identical flow and static conditions, confirm that the effective path length is 90±7 cm and that the ratios of estimated to experimentally measured concentrations are not significantly different from one.

A Nd:YAG laser (Continuum, Surelite II-10) operating at 355 nm is used to initiate CH_2OO production by photolysis of precursor CH_2I_2 in the presence of excess O_2. The photolysis laser is steered through the flow reactor using long-pass dichroics (Semrock, RazorEdge LPD01-335RS). Additional long-pass filters (Semrock, EdgeBasic BLP01-355R) prevent any scattered laser light from reaching either the spectrograph or pulsed LED driver (described below). Typical pulse energies are ~10 mJ in a 7 mm diameter beam, resulting in fluences of ~26 mJ cm^{-2}. The CH_2I_2 absorption cross section at 355 nm ($\sigma_{355} = 5.0\times10^{-19}$ cm^2) is effectively independent of temperature,[40,41] and we estimate that <2% of the CH_2I_2 molecules are photolyzed. Peak concentrations of $[CH_2OO] \approx 1\times10^{13}$ cm^{-3} (measured as described below) are observed approximately 20 μs after photolysis, consistent with the expected pressure-dependent yield and rate of the $CH_2I + O_2$ reaction.[42–44]

Transient absorption spectra are recorded in the wavelength range 360–390 nm as a function of delay time between photolysis and probe ($\Delta t = t_{LED} - t_{355}$). Broadband probe light pulses (200 ns duration) are generated using a pulsed LED driver (LightSpeed Technologies, HPLS-36) fitted with a UV LED centered at 365 nm (approximate FWHM of ~10 nm, maximum output 800 mW). The LED output is highly divergent and is collected using a 2" diameter condenser lens before being focused into 200 μm core multi-mode fiber (NA = 0.22) using a f = 6 cm plano-convex lens. The fiber delivers the LED pulses to the flow reactor where they are approximately collimated using f = 3.5 cm and f = 20 cm lenses and counter-propagated through the flow reactor. The transmitted light is recoupled into an identical fiber and ultimately dispersed in a spectrograph (Andor Shamrock 33i with iDus 420 CCD camera, operated with resolution of 2.5 nm). Synchronization of the photolysis laser, LED, and spectrograph CCD camera) is performed using a digital delay generator (Quantum Composers, 9528) controlled by custom data acquisition software (National Instruments, LabVIEW).

Transient spectra were derived from the average of 400 reference and signal spectra, after subtracting the detector baseline from each. Reference spectra were recorded with delay $\Delta t = t_{\mathrm{LED}} - t_{355} = -10$ μs (i.e. the LED probe pulse is before the laser photolysis pulse), and signal spectra obtained at various (typically ~15) delays spread across the range Δt = 2–2000 μs. Kinetics measurements were performed under pseudo-1st order conditions of excess reactant ([X] at least 30 times greater than $[CH_2OO]_0$) by recording transient blanks ([X] = 0) and using five choked-flow orifices to vary [X]. The choked-flow orifices were selected randomly in each run to minimize the effects of any systematic changes in experimental conditions (e.g. drift in photolysis laser pulse energy or degradation of the reactor windows).

Electronic structure calculations on CH_2OO reaction pathways for acetone (Ac), biacetyl (BiAc), and the enolone tautomer of acetylacetone (AcAc) were performed with *Gaussian 16*.[45] Equilibrium and transition state structures were optimized within the CBS-QB3 compound method that utilizes the B3LYP functional for geometry optimization.[46] The structures obtained are then used for complete basis limit extrapolation based on coupled cluster calculations in CBS-QB3. Minima and transition states were confirmed by harmonic frequency analysis. This level of theory was chosen as it has been shown to provide reliable thermochemistry for reactions involving the main group elements at modest computational cost.[47–49] Cartesian coordinates and images of the optimized geometries of minima and transition states can be found in the Supplementary Material.

Results

Experimental kinetics measurements

The kinetics of the reactions of CH_2OO with acetone, biacetyl, and acetylacetone were studied at a total pressure of 80 Torr and at the temperatures 275 K, 295 K, 315 K, and 335 K.

$$CH_2OO + Ac \rightarrow SOZ \qquad k_{Ac} \qquad \text{(R1)}$$

$$CH_2OO + BiAc \rightarrow SOZ \qquad k_{BiAc} \qquad (R2)$$

$$CH_2OO + AcAc \rightarrow \text{products} \qquad k_{AcAc} \qquad (R3)$$

All kinetics measurements were performed under pseudo-1st order conditions of excess carbonyl ([X] ≫ $[CH_2OO]_0$, by factors of 30–3000). Transient absorption spectra in the range 362–395 nm are decomposed by fitting to a linear combination of reference CH_2OO and IO absorption spectra to obtain time-dependent concentrations $[CH_2OO]_t$ (and $[IO]_t$), as described in our previous work.[26,38,39] Maximum concentrations of $[CH_2OO]_0 \approx (6–8)\times10^{12}$ cm^{-3} are typically observed around 20 μs after photolysis and the increased loss rate due to the presence of the carbonyl compound is evident. The time required to reach the maximum concentration is minimally affected by the presence of Ac, BiAc, or AcAc reactants, although CH_2OO yields are generally lower at higher temperatures.

The kinetic model for loss of CH_2OO includes bimolecular self-reaction, characterized by a rate constant k_{self}, and pseudo-1st order loss, with rate constant k_{loss}. The differential rate equation for CH_2OO loss is

$$\frac{d[CH_2OO]}{dt} = -k_{loss}[CH_2OO] - 2k_{self}[CH_2OO]^2 \qquad E1$$

which can be solved to yield an integrated rate equation

$$[CH_2OO]_t = \frac{k_{loss}[CH_2OO]_0}{k_{loss}\exp(k_{loss}t) - 2k_{self}[CH_2OO]_0[1 - \exp(k_{loss}t)]} \qquad E2$$

that can be used to fit the $[CH_2OO]_t$ data. Unconstrained fits of the experimental data to Equation E2 are not generally reliable, however, particularly when the self-reaction makes comparatively small contribution to CH_2OO loss, which tends to be the case at lower $[CH_2OO]_0$. Neglect of the self-reaction reduces the integrated rate equation for $[CH_2OO]_t$ to a simple exponential decay. Consequently, curvature in plots of $\ln[CH_2OO]_t$ against Δt is evidence of non-negligible contribution from the self-reaction.

In our previous work, we have fixed k_{self} to a previously reported value during fitting. The NASA-JPL evaluation[50] recommends a value of k_{self} = 7.12×10^{-11} cm^3 s^{-1}, which is the average of several measurements all made near room temperature.[43,51,52] In order to explore any possible temperature dependence of k_{self}, we measured transient absorption spectra in the absence of any CI scavenger at 275 K and 335 K. Increasing the laser fluence increases $[CH_2OO]_0$ and consequently leads to a larger contribution of the self-reaction to the CH_2OO loss. At photolysis pulse energies > 10 mJ, plots of

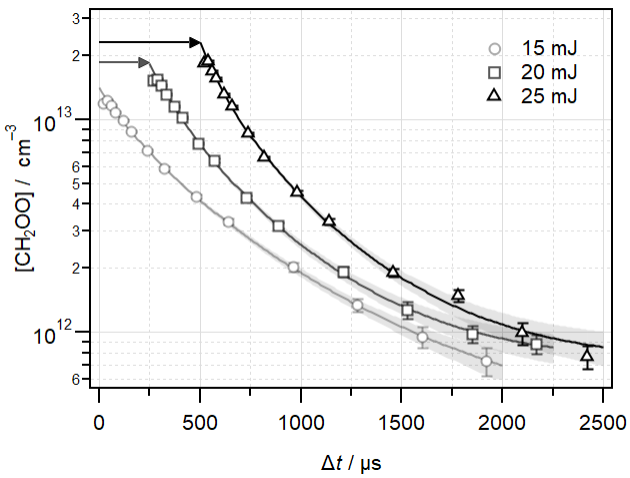

Figure 1 Laser fluence dependence of $[CH_2OO]_t$ at 335 K to show increasing $[CH_2OO]_0$ and increasing curvature at 15 mJ (light gray circles), 20 mJ (gray squares), and 25 mJ (black triangles). Fits to determine k_{loss} and k_{self} are also shown, with shading representing 1σ prediction bands. Data and fits are sequentially offset horizontally for clarity (+250 μs), indicated by the horizontal arrows

$\ln[CH_2OO]_t$ against Δt become increasingly curved (see Figure 1) and fitting to Equation E2 is able to reliably return values for both k_{loss} and k_{self}. The value of k_{loss} increases with laser fluence, consistent with the suggestion that a photochemical product contributes to reactive CH_2OO loss and is generally lower at the higher temperature, for the equivalent laser fluence. In contrast, the values of k_{self} are independent of laser fluence and temperature. We find a value of k_{self} = (7.6±0.8)×10^{-11} cm^3 s^{-1} at 275 K and (8.2±0.5)×10^{-11} cm^3 s^{-1} at 335 K. Combining this value with previous measurements[43,51,52] gives

a temperature-independent weighted average value of k_{self} = (7.8±0.4)×10^{-11} cm^3 s^{-1}. This value is used in all subsequent fits of experimental $[CH_2OO]_t$ time profiles using Equation E2.

Figure 2 shows CH_2OO loss rates obtained at 275 K and 335 K that confirm the linear increase of k_{loss} with increasing carbonyl concentration [X], as expected for pseudo-1st order conditions. The complete data set, including measurements at 295 K and 315 K, is compiled in Supplementary Material as Figures S3–S5. Linear fits of the experimental k_{loss} data as a function of [X] return the bimolecular rate constants, k_X, and a background loss rate, k_0 according to:

$$k_{\text{loss}} = k_0 + k_{\text{X}}[\text{X}] \qquad \text{E3}$$

The T-dependent bimolecular rate constants obtained from an overall fit to three independent

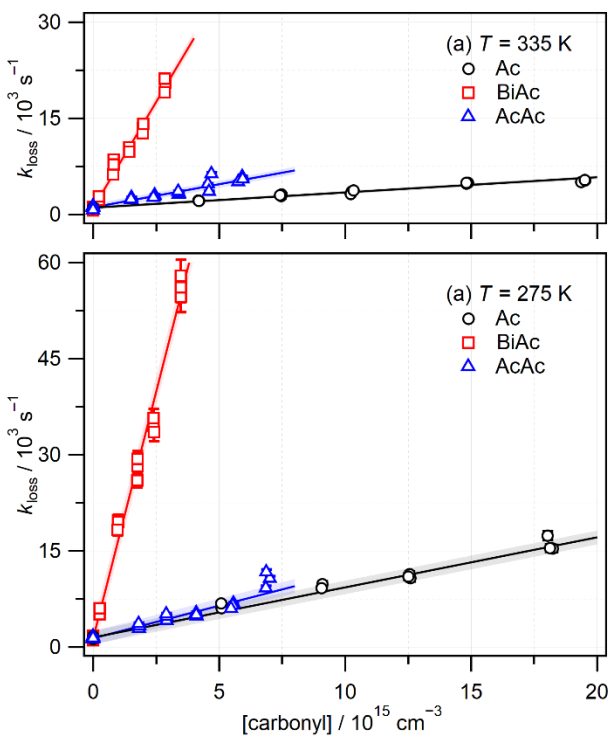

Figure 2 Pseudo-1st order plots of observed k_{loss} against reactant concentration at (a) 335 K and (b) 275 K for the reactions of CH_2OO with Ac (black circles), BiAc (red squares), and AcAc (blue triangles).

Table 2 Temperature-dependent bimolecular rate constants ($\times 10^{-13}$ cm^3 s^{-1}) for the reactions of CH_2OO with Ac, BiAc, and AcAc at 80 Torr. Reported errors are 1σ based on estimated 8% uncertainties in the reactant concentration and statistical uncertainties from the fits.

T / K	k_{Ac}	k_{BiAc}	k_{AcAc}
275	7.8±0.6	154±12	10.2±0.8
295	4.8±0.4	110±9	8.0±0.7
315	3.3±0.3	89±7	8.7±0.7
335	2.4±0.2	66±5	7.2±0.6

kinetics runs are summarized in Table 2, where the reported error bars (1σ) combine the statistical from the linear fits and an estimated 8% uncertainty in the reactant concentrations derived from calibration measurements. The *T*-dependent rate constants for the CH_2OO + BiAc reaction ($\sim 10^{-11}$ cm^3 s^{-1}) are markedly larger than those for the CH_2OO + Ac and CH_2OO + AcAc reactions ($\sim 10^{-13}$–10^{-12} cm^3 s^{-1}) across the temperature range and all three reactions show a negative temperature dependence. The background CH_2OO loss rates also decrease with increasing temperature (k_0 is approximately 1500 s^{-1} at 275 K and 1000 s^{-1} at 335 K). Arrhenius plots, shown in Figure 3, are linear over the experimental temperature range. The pre-exponential factors and activation energies derived from linear fits are summarized in Table 3. The sensitivity of $k(T)$ to changes in temperature decreases in the order Ac > BiAc > AcAc, as indicated by the smaller magnitude of E_a. The pre-exponential factors suffer from significant statistical uncertainty, particularly for the Ac and BiAc reactions.

The kinetics of the CH_2OO + Ac reaction has been studied by several groups previously and the results

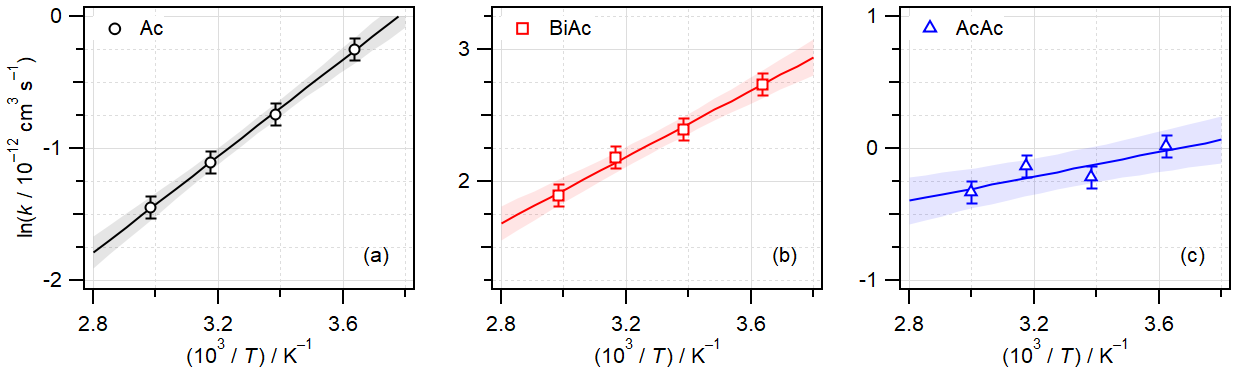

Figure 3 Arrhenius plots for the reactions of CH_2OO with (a) Ac (black circles), (b) BiAc (red squares), and (c) AcAc (blue triangles) over the temperature range 275–335 K. Shaded areas represent 1σ prediction bands for the linear fits. Fit parameters are summarized in **Error! Reference source not found.**.

are summarized in Table 1.[21–23,25,26] The value of k_{Ac} = (4.8±0.4)×10^{-13} cm^3 s^{-1} at 295 K obtained in this work agrees well with our previous measurement[26] and, where temperature ranges overlap, the agreement with the values reported by Chhantyal-Pun et al.[25] across the range 251–311 K is excellent. In contrast, Taatjes et al.[21] at 296 K and Elsamra et al.,[23] across the range 298-494 K, found rate constants that are around a factor of two smaller. As argued by Chhantyal-Pun et al., the discrepancy

Table 3 Arrhenius and thermodynamic parameters for rate-limiting TS.

	Ac	BiAc	AcAc
A / cm^3 s^{-1}	(1.0±0.5)×10^{-15}	(1.6±0.9)×10^{-13}	(1.8±1.1)×10^{-13}
E_a / kcal mol^{-1}	−3.6±0.3	−2.5±0.3	−0.9±0.3
(E_a / R) / K	−1830±170	−1260±170	−460±180
ΔS° / cal K^{-1} mol^{-1}	−42.5±1.1	−32.1±1.2	−32.4±1.1
ΔH° / kcal mol^{-1}	−4.8±0.3	−2.1±0.4	−3.7±0.3

is likely attributable to the different bath gas and pressure conditions used in the earlier experiments. As in the current experiments, Chhantyal-Pun et al. used N_2 bath gas and furthermore they showed that the high-*P* limit had been reached by ~30 Torr. A series of experiments performed to measure CH_2OO loss rates in the presence of a fixed concentration of Ac showed no pressure dependence across the range 50–100 Torr. Consequently, we conclude that the results of the current experiments at 80 Torr N_2 are also performed under conditions that correspond to the high-*P* limit and are directly comparable to the results of Chhantyal-Pun et al. The earlier measurements by Taatjes et al. and Elsamra et al. used He and were performed at lower pressures (4 Torr and < 25 Torr, respectively);[21,23] a weak positive pressure dependence was observed by the latter group, suggesting the high-*P* limit may not have been reached. The rate constant measured at 297 K and in 1 atm air by Berndt et al.[22] should also be at the high-*P* limit. The value reported is slightly smaller than more recent values,[25,26] but agrees within the mutual experimental uncertainties.

To the best of our knowledge, the only previous report of the kinetics of the reactions of CH_2OO with BiAc and AcAc is our recent study at 295 K.[26] For the BiAc reaction, the value of the rate constant at 295 K of $(1.10\pm0.09)\times10^{-11}$ cm^3 s^{-1} is smaller than the previous value of $(1.45\pm0.18)\times10^{-11}$ cm^3 s^{-1} (1σ uncertainties). In contrast, the current value of the rate constant for the AcAc reaction of $(8.0\pm0.7)\times10^{-13}$ cm^3 s^{-1} is larger than our previous measurement of $(6.6\pm0.6)\times10^{-13}$ cm^3 s^{-1}. Although there is an apparent disagreement, we note that the measurements agree within 2σ uncertainty. We consider the current results to be more reliable. Background CH_2OO loss rates in the current work were significantly slower (~1300 s^{-1} at 295 K in the current work compared to ~4000–6000 s^{-1} in Cornwell et al.[26]) and the pseudo-1st order plots span a greater range of k_{loss}. As with the CH_2OO + Ac reaction, a series of measurements of CH_2OO loss rates with known concentrations of BiAc and Ac were performed at total pressures in the range 50–100 Torr (see Figure S6 in the Supplementary Information). No pressure dependence was observed, and we conclude that these reactions are either pressure-independent or, more likely, also taking place at the high-*P* limit.

Computational Results

Cycloaddition at the carbonyl group

The cycloaddition reactions between CH_2OO and Ac, BiAc, and AcAc at the carbonyl group were characterized in our previous work.[26] Here, we expand on those results and correct a minor error in the 0 K energies reported in that publication. The reaction pathway for cycloaddition at the carbonyl group consists of an entrance channel van der Waals complex before reaching a transition state barrier that leads to the secondary ozonide. However, recent work has shown that another complex and transition state pair at further reactant separation can also play an important role in these reactions.[31] Therefore, we have also characterized what will be referred to as the *outer* complex

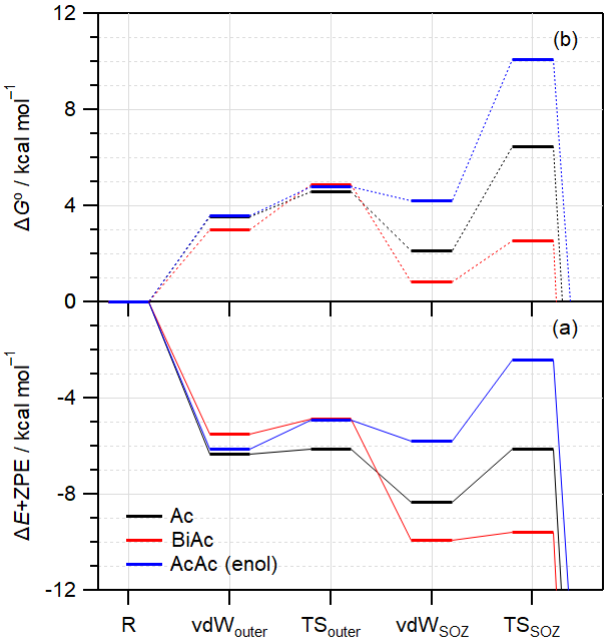

Figure 4 Stationary point (a) energies at 0 K (ΔE+ZPE, solid lines) and (b) free energies at 298 K ($\Delta G°$, dotted lines) cycloaddition reactions of CH_2OO with acetone (Ac, black), biacetyl (BiAc, red), and the enol tautomer of acetylacetone (AcAc, blue) to form a secondary ozonide (SOZ). Geometries are shown in Supplementary Information.

(vdW_{outer})and transition state (TS_{outer}) in addition to the *inner* complex (vdW_{SOZ}) and transition state (TS_{SOZ}) that lead to SOZ products that were characterized previously. The reaction pathways with 0 K energies (ΔE+ ZPE) and standard Gibbs free energies ($\Delta G°$) at 298 K are shown in Figure 4 and tabulated in **Error! Reference source not found.**. The 0 K ΔE+ZPE results presented here for the CH_2OO + Ac reaction are identical to the CBS-QB3 values reported by Wang et al.[31]

The 0 K energy profiles in Figure 4(a) show that the long-range complex vdW_{outer} lies around 4 kcal mol^{-1} lower than the reactants for all three reactions. TS_{outer} presents only a modest energy barrier <2 kcal mol^{-1} to rearrangement to vdW_{SOZ}, which lies to lower energy than vdW_{outer} for the Ac and BiAc reactions. For the Ac and AcAc reactions the five-membered cyclic transition state for SOZ formation, TS_{SOZ} is around +2 to +5 kcal mol^{-1} higher in energy relative to vdW_{SOZ}, but only +0.3 kcal mol^{-1} for the BiAc reaction. On the 0 K energy surfaces, TS_{SOZ} presents the largest barrier (relative to the previous complex) for the Ac and AcAc reactions, while TS_{outer} is the largest barrier for the BiAc

Table 4 Relative energies (ΔE+ZPE at 0 K), including zero-point contributions, and free energies ($\Delta G°$ at 298 K), calculated at the CBS-QB3 levels for the SOZ pathway (see Figure 4) for reactions of CH_2OO with acetone (Ac), biacetyl (BiAc), and the enolone tautomer of acetylacetone (AcAc). All energies are reported in kcal mol^{-1}.

	Ac	BiAc	AcAc
vdW_{outer}	−6.3 (+3.5)	−5.5 (+3.0)	−6.1 (+3.6)
TS_{outer}	−6.1 (+4.6)	−4.9 (+4.9)	−4.9 (+4.8)
vdW_{SOZ}	−8.3 (+2.1)	−9.9 (+0.8)	−7.5 (+2.9)
TS_{SOZ}	−6.1 (+6.5)	−9.6 (+2.5)	−2.4 (+10.1)
SOZ	−50.3 (−36.6)	−50.1 (−37.0)	−39.2 (−25.9)

reaction. The equivalent $\Delta G°$ reaction profiles are shown in Figure 4(b). The reaction profiles are similar for the three reactions up to TS_{outer}, at around +5 kcal mol^{-1} but diverge beyond. For the BiAc reaction, TS_{outer} is the highest point on the free energy surface, and is likely rate-limiting, while TS_{SOZ} is significantly higher in energy for the Ac and AcAc reactions.

Alternate pathways for the enolone tautomer of AcAc

The enolone tautomer of AcAc has more possible reaction sites than Ac and BiAc given the presence of the C=C double bond and the O–H functional group. Therefore, it is of interest to identify if other reaction pathways are contributing to the measured reaction rate in addition to cycloaddition at the carbonyl group. We have identified four additional transition states that are representative of the major reaction pathways but neglect subtle conformational differences that would lead to TSs with very similar energies. These new transition states correspond to two cycloadditions at the C=C group involving different orientations of CH_2OO (O atom of the CI adding either to the α–C or β–C atom, labelled as C_α=C and C_β=C, respectively), a cycloaddition via a seven-membered transition state that

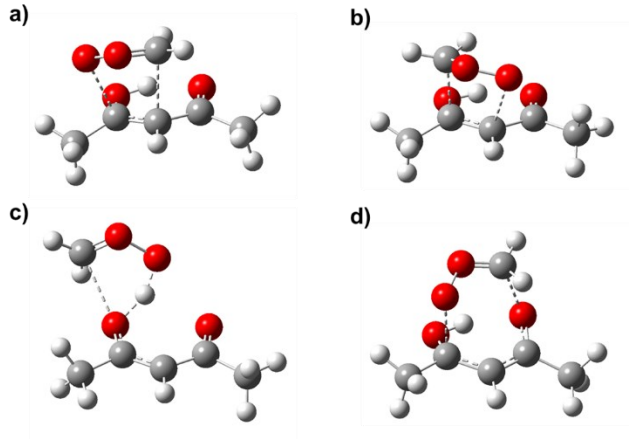

Figure 5 Transition state structures for reactions of the enolone tautomer of AcAc. (a) Cycloaddition at the C=C bond with O atom attack at the β-C atom; (b) cycloaddition at the C=C bond with O atom attack at the α-C atom; (c) 1,2-addition at the OH group; and (d) cycloaddition via a seven-membered cyclic adduct involving the carbonyl O atom and β-C atom.

involves the carbonyl O atom and the β–C atom(labelled C_β=C–C=O), and a 1,2-addition (1,2-insertion, labelled OH) of the CI across the CH_2OO, typical of reactions with simple alcohols.[39,53,54] These transition state structures are shown in Figure 5 and the Δ*E*+ZPE at 0 K and Δ*G*° at 298 K values for the TSs and the direct products that result are compiled in **Error! Reference source not found.**. Cartesian coordinates for each TS structure optimized within the CBS-QB3 compound method are included in the Supplementary Material. In comparison to reaction at the carbonyl group, reaction at the C=C double bond would be expected to be the most competitive. In fact, reaction in the C_β=C orientation has a free energy barrier that is equivalent to that for reaction at the C=O group (discussed further below) However, reaction at the OH group and the cycloaddition reactions involving the C_α=C orientation and the seven-membered TS are likely minor channels given that their free energies barriers are significantly higher.

Table 5 Relative energies (Δ*E*+ZPE at 0 K), including zero-point contributions, and free energies (Δ*G*° at 298 K) calculated at the CBS-QB3 levels for all reaction pathways for the enolone tautomer of acetylacetone (AcAc). TS energies are for the inner transition states (see Figure 5). All energies are reported in kcal mol^{-1}.

Reaction Site	Δ*E*+ZPE (Δ*G*°)	
	TS	Products
C=O	–2.4 (+10.1)	–39.2 (–25.9)
C_β=C	–2.3 (+10.1)	–53.1 (–39.9)
C_α=C	+3.3 (+16.1)	–46.6 (–33.6)
OH	+9.8 (+20.9)	–36.0 (–24.0)
C_β= C_α–C=O	+10.4 (+23.4)	–39.8 (–26.1)

It is interesting that the C_α=C and C_β=C isomeric reaction pathways differ so much in relative energy (> 5 kcal mol^{-1}). The difference between the isomers is likely due to two effects. Firstly, there is more steric hinderance between the CH_2 group of CH_2OO and the terminal methyl group of AcAc that is not present in the C_β=C transition state. In addition to the steric effects, natural bond orbital (NBO) analysis on the enolone tautomer of AcAc reveals that the β–C atom is more electropositive than the α–C atom which can result in a more favorable interaction with the electronegative terminal oxygen atom in CH_2OO.

Discussion

The major experimental result is the clear negative temperature dependences of all three reactions studied over the range 275–315 K. The linear Arrhenius plots shown in Figure 3 and activation energies collated in **Error! Reference source not found.** indicate that the sensitivity to temperature decreases in order Ac > BiAc > AcAc. The CH_2OO + Ac reaction is independent of the pressure of N_2 bath gas over the range 50–100 Torr, consistent with earlier work that found the high-pressure limit had been reached by 30 Torr.[25] The rates of the BiAc and AcAc reactions also appear to be independent of pressure over the same range and consequently are assumed to also be taking place in the high-*P* limit regime. In the gas phase, AcAc exists as a mixture of diketone and enolone tautomers, with the latter being strongly favored.[55–57] Using the enthalpy and entropy changes from the van't Hoff analysis reported by Antonov et al.,[57] the mole fraction of the dominant enolone tautomer decreases only slightly from 0.983 to 0.941 across the experimental temperature range. Since the *ab initio* results described above do not suggest any reason to expect the minor diketone to react significantly more rapidly than the enolone, we assume in the following discussion that all reactivity is due to the latter.

While previous work on the cycloaddition of CIs to carbonyls has largely focused on the inner vdW complex and TS as the rate-determining step in this reaction, recent work by Wang et al. has shown

that the long-range outer vdW complex and TS can be rate-limiting in some cases.[31] For instance, in the reaction of CH_2OO and CH_3CHO, the energy barriers for the outer complex and TS are higher energy and were shown to determine the overall rate. Here, the reaction profile for BiAc (Figure 4) is like that of acetaldehyde, suggesting that the overall reaction rate is dictated by TS_{outer}. For Ac and AcAc, the rate limiting step is expected to be passage over the inner TS_{SOZ}, although for the latter, other reaction pathways may be competitive.

Reactions between CIs and carbonyls are thought to proceed via the following two-step mechanism in the high-*P* limit:[23,25]

$$CH_2OO + X \rightleftharpoons vdW \qquad k_1/k_{-1}$$

$$vdW \rightarrow product \qquad k_2$$

The highly exothermic second step is a 1,3-cycloaddition reaction that forms the cyclic 1,2,4-trioxolane SOZ product. The notation vdW refers to the complex prior to the rate-limiting TS, viz. the *inner* complex for Ac and AcAc, and the *outer* complex for BiAc. Application of the steady state approximation to the vdW complex leads to an expression for the overall reaction rate wherein the observed second order rate constant is

$$k_{\text{obs}} = \frac{k_2 k_1}{k_{-1} + k_2} \qquad \text{E4}$$

If the second step is rate limiting (i.e. in the limit that $k_{-1} \gg k_2$), a fast equilibrium between the reactants and the entrance channel vdW complex is established and the expression for the observed rate constant will be reduced to

$$k_{\text{obs}} = k_2 \frac{k_1}{k_{-1}} = k_2 K_1 \qquad \text{E5}$$

While this limit seems reasonable for the Ac and AcAc reactions, for which TS_{in} lies at a significantly higher energy than the most stable complex, vdW_{in}, the same cannot be said for the BiAc reaction,

where the small barriers suggest that k_2 is likely to be large (see Figure 4 and **Error! Reference source not found.**). However, in the alternative limit that $k_2 \gg k_{-1}$, the expression for the observed rate constant reduces to that of formation of the relevant vdW complex and

$$k_{\text{obs}} = k_1 \qquad \text{E6}$$

The value of k_2 can be readily calculated using the results of the CBS-QB3 calculations and applying canonical transition state theory (CTST). Similarly, we can estimate the value of k_{-1} using the theoretical value for K_1 and estimating k_1. Upper limits for k_1 (and hence lower limits for k_{-1}) can be estimated using a simple hard-sphere collision rate, k_{hs}. Using $k_1 \approx k_{\text{hs}}$, we estimate that the ratio k_{-1}/k_2 has values of order 10^5, 10^2, and 10 for AcAc, Ac, and BiAc, respectively, with the values increasing with temperature. Consequently, based on the two-step high-P limit model and the discussion above, we assume that the observed experimental rate constant represents the product of k_2 and the equilibrium constant K_1. Applying CTST to k_2 leads to the expression[25]

$$k_{\text{obs}}(T) = \frac{k_B^2}{hp^\circ} \exp\left(\frac{\Delta S^\circ}{R}\right) T^2 \exp\left(-\frac{\Delta H^\circ}{RT}\right) \qquad \text{E7}$$

where the values of ΔS° and ΔH° correspond to the change from the reactants to the highest point on the free energy surface (ΔG°). For the Ac and AcAc reactions, that corresponds to TS_{SOZ}, while for the BiAc reaction it is TS_{outer} (see Figure 4 and **Error! Reference source not found.**). The factor k_B^2/hp° is evaluated to be 2.84×10^{-12} cm^3 s^{-1} K^{-2} using p° = 101325 Pa. We fit the experimental T-dependent rate constants to the expression

$$k_{\text{obs}}(T) = AT^2 \exp(-B/T) \qquad \text{E8}$$

where the parameters A and B can be related to the entropy and enthalpy via Equation E7. The fits are shown in Figure 6 and the thermodynamic variables obtained are compiled in Table 2.

Comparing the experimental values of $\Delta S°$ and $\Delta H°$ obtained from this analysis to the theoretical values calculated at the CBS-QB3 level of theory, we find a qualitative trend with the theoretical $\Delta H°$ values being slightly more negative by ~1.0 – 2.2 kcal mol^{-1}. For $\Delta S°$, there is excellent agreement for the experimental and theoretical values for Ac and BiAc with Ac exhibiting a significantly more negative value. This is consistent with the expected rate-determining steps for Ac and BiAc based on the reaction profiles in Figure 4. For Ac, formation of the TS_{SOZ} is the rate determining step which is

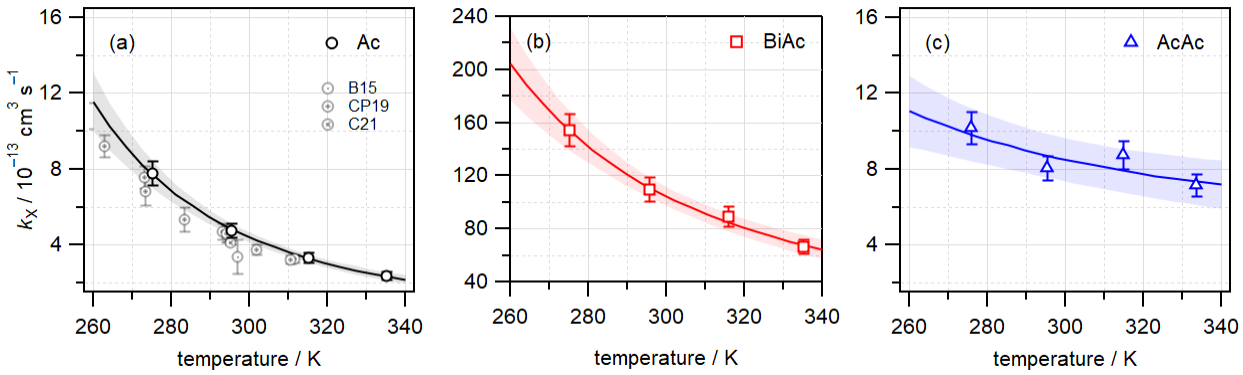

Figure 6 Plots of k_X against T for the reactions of CH_2OO with (a) Ac (black circles), (b) BiAc (red squares), and (c) AcAc (blue triangles). The solid lines are fits to Equation E8 (see text), used to extract thermodynamic parameters for the rate-limiting TS. Shaded areas represent 1σ prediction bands. Previous high-P limit measurements in this temperature range from Berndt et al.[22] (B15, gray circle with dot), Chhantyal-Pun et al.[25] (CP19, gray circle with plus), Cornwell et al.[26] (C21, gray circle with cross) are also shown.

a tighter (more ordered, higher vibrational frequencies) structure than the TS_{outer} that occurs at larger reactant separation. The opposite is true of BiAc where the rate-determining step is passage over the looser, higher entropy TS. In contrast, the experimental value of $\Delta S°$ for AcAc differs substantially from the theoretical value. Given that the rate-determining step for AcAc is the formation of TS_{SOZ}, it would be expected to have a more negative $\Delta S°$ similar to that of Ac. However, the $\Delta S°$ is much closer to the value for BiAc. The higher-than-expected entropy for AcAc may be due

to the contributions of multiple available reaction pathways (Figure 5), discussed below.

Multiple reaction pathways are possible for the reaction of CH_2OO with the dominant enolone tautomer of AcAc, which shows the weakest *T* dependence of the reactions studied. The CBS-QB3 calculations find the smallest, and equivalent, free energy barriers at 298 K for cycloaddition at both the C=O and C_β=C sites (Table 5), while reaction at the OH group or other sites is uncompetitive. Previously, reactions of CH_2OO with alkenes have been shown to have rate constants that are significantly smaller than acetone but with a positive temperature dependence.[37] The overall weak *T* dependence observed for the AcAc reaction may reflect the balance between the expected positive and negative *T* dependences of the rate constants for reaction at the C=C and C=O sites, respectively. This interpretation would imply that reactivity at the C_β=C site is significantly enhanced over that of simple alkenes, perhaps enhanced by the presence of the OH group in the enolone tautomer of AcAc. Previous work with the ozonolysis of alkenes, which proceeds via a similar cycloaddition mechanism, has shown that nearby OH groups enhance the rate of reaction.[58] We note that the conjugated π-system in AcAc is akin to the α,β-unsaturated carbonyl moiety found in species such as MVK, MACR, and ACR for which the kinetics of reactions with CH_2OO have also been studied.[24,32] PIMS measurements from Eskola *et al.*[24] confirmed the formation of the 1,2,4-trioxolane SOZ species in the MVK and MACR reactions, and it was concluded that the reactions proceed near exclusively through cycloaddition at the C=O at room temperature. Further experimental work identifying the products of the CH_2OO + AcAc reaction would be required to confirm that both reaction mechanisms are indeed competitive given that the theoretical $\Delta G°$ values indicate that both pathways will occur.

In the troposphere, the major daytime removal process for BiAc and AcAc is photolysis, which dominates over reaction with atmospheric oxidants such as OH or CH_2OO, and results in lifetimes of only a few hours.[59,60] Photolysis is far slower for Ac,[61] but still the most important sink. Consequently, reactive sinks primarily contribute at nighttime when temperatures are also lower. For AcAc, the rate constant for reaction with OH is significantly larger than that for CH_2OO, and also shows a stronger

negative temperature dependence (E_a/R = –980 K for OH + AcAc).[62] Consequently, reaction with OH becomes increasingly important relative to CH_2OO as temperature decreases. In contrast, the reactions of OH with Ac (E_a/R = +1320 K)[63] and BiAc (E_a/R = +450 K)[64] both have positive temperature dependences. Loss due to reaction with CH_2OO may become relatively more important at nighttime, when both the temperature and the OH concentration are lower. Figure 7 shows the ratio of Ac and BiAc loss rates due to reaction with OH and CH_2OO as a function of temperature for day and night. Atmpospheric concentrations of CH_2OO have been estimated to span the range (1–10)×10^4 cm^{-3};[8,65] the calculations use a estimated value of 2×10^4 cm^{-3}, while the value of [OH] is estimated to be 5×10^6 cm^{-3} during the day and 2×10^5 cm^{-3} at night.[66,67] OH is a more important reactive sink than CH_2OO in the daytime for both Ac and BiAc across the 220–320 K temperature range. Nighttime loss rates due to reaction with CH_2OO are larger at all temperatures for BiAc, and at T < 260 K for Ac.

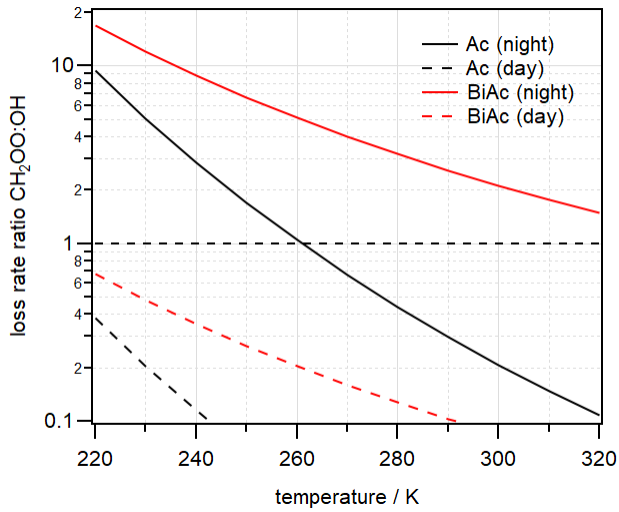

Figure 7 Temperature dependence of the ratio of Ac (black) and BiAc (red) loss rates due to reaction with CH_2OO and OH. Calculated ratios based on estimated approximate daytime (dashed lines) and nighttime (solid lines) concentrations of CH_2OO and OH are shown.

Conclusions

The *T*-dependent kinetics of the reactions of CH_2OO with Ac, BiAc, and AcAc have been measured over the range 275–335 K at total pressure of 80 Torr, which corresponds to the high-*P* limit. The measured rate constants are in good agreement with previous measurements performed under similar conditions.[25] All three reactions show a negative temperature dependence, with rate constants increasing at lower temperature. Characterization of the key stationary points on the reaction potential energy (and free energy) surfaces, suggests that the rate limiting step for the fast BiAc reaction is a long-range re-orientation TS, akin to that identified in the CH_2OO + acetaldehyde reaction.[31] In contrast, the short-range cycloaddition TS is rate-limiting for the slower Ac and AcAc reactions. Four new reaction pathways have been identified computationally for the AcAc reaction, with cycloaddition at the C_β=C site being competitive with the analogous reaction at the C=O site. Work is underway to expand the available experimental kinetic data set to include other multifunctional VOCs, with a goal of developing SARs with predictive power, analogous to those that have been used for alkene ozonolysis.[58,68–72] For Ac and BiAc, the negative temperature dependence suggests that CH_2OO could be a more significant reactive sink than OH at night, when concentrations of the latter are lower and photolysis is absent.

Acknowledgements

This material is based upon work supported by the National Science Foundation under Grant No. ECS-1905364.

References

1. Criegee R. Mechanism of Ozonolysis. *Angew Chem Int Ed Engl*. 1975;14(11):745-752. doi:10.1002/anie.197507451
2. Hatakeyama S, Akimoto H. Reactions of Criegee Intermediates in the Gas Phase. *Res Chem Intermed*. 1994;20(3-5):503-524. doi:10.1163/156856794X00432
3. Johnson D, Marston G. The gas-phase ozonolysis of unsaturated volatile organic compounds in the troposphere. *Chem Soc Rev*. 2008;37(4):699-716. doi:10.1039/B704260B
4. Donahue NM, Drozd GT, Epstein SA, Presto AA, Kroll JH. Adventures in ozoneland: down the rabbit-hole. *Phys Chem Chem Phys*. 2011;13(23):10848-10857. doi:10.1039/C0CP02564J
5. Taatjes CA, Shallcross DE, Percival CJ. Research frontiers in the chemistry of Criegee intermediates and tropospheric ozonolysis. *Phys Chem Chem Phys*. 2014;16(5):1704-1718. doi:10.1039/C3CP52842A
6. Osborn DL, Taatjes CA. The physical chemistry of Criegee intermediates in the gas phase. *Int Rev Phys Chem*. 2015;34(3):309-360. doi:10.1080/0144235X.2015.1055676
7. Taatjes CA. Criegee Intermediates: What Direct Production and Detection Can Teach Us About Reactions of Carbonyl Oxides. *Annu Rev Phys Chem*. 2017;68(1):183-207. doi:10.1146/annurev-physchem-052516-050739
8. Khan MAH, Percival CJ, Caravan RL, Taatjes CA, Shallcross DE. Criegee intermediates and their impacts on the troposphere. *Environ Sci: Processes Impacts*. 2018;20(3):437-453. doi:10.1039/C7EM00585G
9. Cabezas C, Nakajima M, Endo Y. Criegee intermediates meet rotational spectroscopy. *Int Rev Phys Chem*. 2020;39(3):351-384. doi:10.1080/0144235X.2020.1782651
10. Chhantyal-Pun R, Khan MAH, Taatjes CA, Percival CJ, Orr-Ewing AJ, Shallcross DE. Criegee intermediates: production, detection and reactivity. *Int Rev Phys Chem*. 2020;39(3):385-424. doi:10.1080/0144235X.2020.1792104
11. Cox RA, Ammann M, Crowley JN, et al. Evaluated kinetic and photochemical data for atmospheric chemistry: Volume VII – Criegee intermediates. *Atmos Chem Phys*. 2020;20(21):13497-13519. doi:10.5194/acp-20-13497-2020
12. Nguyen TB, Tyndall GS, Crounse JD, et al. Atmospheric fates of Criegee intermediates in the ozonolysis of isoprene. *Phys Chem Chem Phys*. 2016;18(15):10241-10254. doi:10.1039/C6CP00053C
13. Jenkin ME, Clemitshaw KC. Ozone and other secondary photochemical pollutants: chemical processes governing their formation in the planetary boundary layer. *Atmos Environ*. 2000;34(16):2499-2527. doi:10.1016/S1352-2310(99)00478-1
14. Lary DJ, Shallcross DE. Central role of carbonyl compounds in atmospheric chemistry. *J Geophys Res*. 2000;105(D15):19771-19778. doi:10.1029/1999JD901184
15. Khan MAH, Cooke MC, Utembe SR, et al. A study of global atmospheric budget and distribution of acetone using global atmospheric model STOCHEM-CRI. *Atmos Environ*. 2015;112:269-277. doi:10.1016/j.atmosenv.2015.04.056
16. Su F, Calvert JG, Shaw JH. A FT IR spectroscopic study of the ozone-ethene reaction mechanism in oxygen-rich mixtures. *J Phys Chem*. 1980;84(3):239-246. doi:10.1021/j100440a003

17. Neeb P, Horie O, Moortgat GK. The nature of the transitory product in the gas-phase ozonolysis of ethene. *Chem Phys Lett*. 1995;246(1–2):150-156. doi:10.1016/0009-2614(95)01073-I

18. Neeb P, Horie O, Moortgat GK. Formation of secondary ozonides in the gas-phase ozonolysis of simple alkenes. *Tetrahedron Lett*. 1996;37(52):9297-9300. doi:10.1016/S0040-4039(97)82946-2

19. Neeb P, Horie O, Moortgat GK. The Ethene−Ozone Reaction in the Gas Phase. *J Phys Chem A*. 1998;102(34):6778-6785. doi:10.1021/jp981264z

20. Horie O, Schäfer C, Moortgat GK. High reactivity of hexafluoro acetone toward criegee intermediates in the gas-phase ozonolysis of simple alkenes. *Int J Chem Kinet*. 1999;31(4):261-269. doi:10.1002/(SICI)1097-4601(1999)31:4<261::AID-KIN3>3.0.CO;2-Z

21. Taatjes CA, Welz O, Eskola AJ, et al. Direct measurement of Criegee intermediate (CH_2OO) reactions with acetone, acetaldehyde, and hexafluoroacetone. *Phys Chem Chem Phys*. 2012;14(30):10391-10400. doi:10.1039/C2CP40294G

22. Berndt T, Kaethner R, Voigtländer J, et al. Kinetics of the unimolecular reaction of CH_2OO and the bimolecular reactions with the water monomer, acetaldehyde and acetone under atmospheric conditions. *Phys Chem Chem Phys*. 2015;17(30):19862-19873. doi:10.1039/C5CP02224J

23. Elsamra RMI, Jalan A, Buras ZJ, Middaugh JE, Green WH. Temperature- and Pressure-Dependent Kinetics of CH_2OO + CH_3COCH_3 and CH_2OO + CH_3CHO: Direct Measurements and Theoretical Analysis. *Int J Chem Kinet*. 2016;48(8):474-488. doi:10.1002/kin.21007

24. Eskola AJ, Döntgen M, Rotavera B, et al. Direct kinetics study of CH_2OO + methyl vinyl ketone and CH_2OO + methacrolein reactions and an upper limit determination for CH_2OO + CO reaction. *Phys Chem Chem Phys*. 2018;20(29):19373-19381. doi:10.1039/C8CP03606C

25. Chhantyal-Pun R, Khan MAH, Martin R, et al. Direct Kinetic and Atmospheric Modeling Studies of Criegee Intermediate Reactions with Acetone. *ACS Earth Space Chem*. 2019;3(10):2363-2371. doi:10.1021/acsearthspacechem.9b00213

26. Cornwell ZA, Harrison AW, Murray C. Kinetics of the Reactions of CH_2OO with Acetone, α-Diketones, and β-Diketones. *J Phys Chem A*. 2021;125(39):8557-8571. doi:10.1021/acs.jpca.1c05280

27. Cremer D, Kraka E, McKee ML, Radharkrishnan TP. The carbonyl oxide-aldehyde complex: a new intermediate of the ozonolysis reaction. *Chem Phys Lett*. 1991;187(5):491-493. doi:10.1016/0009-2614(91)80288-9

28. Aplincourt P, Ruiz-López MF. Theoretical Study of Formic Acid Anhydride Formation from Carbonyl Oxide in the Atmosphere. *J Phys Chem A*. 2000;104(2):380-388. doi:10.1021/jp9928208

29. Aplincourt P, Ruiz-López MF. Theoretical Investigation of Reaction Mechanisms for Carboxylic Acid Formation in the Atmosphere. *J Am Chem Soc*. 2000;122(37):8990-8997. doi:10.1021/ja000731z

30. Jalan A, Allen JW, Green WH. Chemically activated formation of organic acids in reactions of the Criegee intermediate with aldehydes and ketones. *Phys Chem Chem Phys*. 2013;15(39):16841-16852. doi:10.1039/C3CP52598H

31. Wang PB, Truhlar DG, Xia Y, Long B. Temperature-dependent kinetics of the atmospheric reaction between CH_2OO and acetone. *Phys Chem Chem Phys*. 2022;24(21):13066-13073. doi:10.1039/D2CP01118B

32. Zhou X, Chen Y, Liu Y, Li X, Dong W, Yang X. Kinetics of CH_2OO and syn-CH_3CHOO reaction with acrolein. *Phys Chem Chem Phys*. 2021;23(23):13276-13283. doi:10.1039/D1CP00492A

33. Sustmann R. A simple model for substituent effects in cycloaddition reactions. I. 1,3-dipolar cycloadditions. *Tetrahedron Lett*. 1971;12(29):2717-2720. doi:10.1016/S0040-4039(01)96961-8

34. Houk KN. Frontier molecular orbital theory of cycloaddition reactions. *Acc Chem Res*. 1975;8(11):361-369. doi:10.1021/ar50095a001

35. Fukui K. Role of Frontier Orbitals in Chemical Reactions. *Science*. 1982;218(4574):747-754. doi:10.1126/science.218.4574.747

36. Hansch Corwin, Leo A, Taft RW. A survey of Hammett substituent constants and resonance and field parameters. *Chem Rev*. 1991;91(2):165-195. doi:10.1021/cr00002a004

37. Buras ZJ, Elsamra RMI, Jalan A, Middaugh JE, Green WH. Direct Kinetic Measurements of Reactions between the Simplest Criegee Intermediate CH_2OO and Alkenes. *J Phys Chem A*. 2014;118(11):1997-2006. doi:10.1021/jp4118985

38. Foreman ES, Kapnas KM, Murray C. Reactions between Criegee Intermediates and the Inorganic Acids HCl and HNO_3: Kinetics and Atmospheric Implications. *Angew Chem Int Ed*. 2016;55(35):10419-10422. doi:10.1002/anie.201604662

39. Tadayon SV, Foreman ES, Murray C. Kinetics of the Reactions between the Criegee Intermediate CH_2OO and Alcohols. *J Phys Chem A*. 2018;122(1):258-268. doi:10.1021/acs.jpca.7b09773

40. Roehl CM, Burkholder JB, Moortgat GK, Ravishankara AR, Crutzen PJ. Temperature dependence of UV absorption cross sections and atmospheric implications of several alkyl iodides. *J Geophys Res*. 1997;102(D11):12819-12829. doi:10.1029/97JD00530

41. Mössinger JC, Shallcross DE, Cox RA. UV-VIS absorption cross-sections and atmospheric lifetimes of CH_2Br_2, CH_2I_2 and CH_2BrI. *J Chem Soc, Faraday Trans*. 1998;94(10):1391-1396. doi:10.1039/A709160E

42. Eskola AJ, Wojcik-Pastuszka D, Ratajczak E, Timonen RS. Kinetics of the reactions of CH_2Br and CH_2I radicals with molecular oxygen at atmospheric temperatures. *Phys Chem Chem Phys*. 2006;8(12):1416-1424. doi:10.1039/b516291b

43. Ting WL, Chang CH, Lee YF, Matsui H, Lee YP, Lin JJM. Detailed mechanism of the $CH_2I + O_2$ reaction: Yield and self-reaction of the simplest Criegee intermediate CH_2OO. *J Chem Phys*. 2014;141(10):104308. doi:10.1063/1.4894405

44. Huang YH, Chen LW, Lee YP. Simultaneous Infrared Detection of the ICH_2OO Radical and Criegee Intermediate CH_2OO: The Pressure Dependence of the Yield of CH_2OO in the Reaction $CH_2I + O_2$. *J Phys Chem Lett*. 2015;6(22):4610-4615. doi:10.1021/acs.jpclett.5b02298

45. Gaussian 16, Revision B.01, Frisch, M. J.; Trucks, G. W.; Schlegel, H. B.; Scuseria, G. E.; Robb, M. A.; Cheeseman, J. R.; Scalmani, G.; Barone, V.; Petersson, G. A.; Nakatsuji, H.; Li, X.; Caricato, M.; Marenich, A. V.; Bloino, J.; Janesko, B. G.; Gomperts, R.; Mennucci, B.; Hratchian, H. P.; Ortiz, J. V.; Izmaylov, A. F.; Sonnenberg, J. L.; Williams-Young, D.; Ding, F.; Lipparini, F.; Egidi, F.; Goings, J.; Peng, B.; Petrone, A.; Henderson, T.; Ranasinghe, D.; Zakrzewski, V. G.; Gao, J.; Rega, N.; Zheng, G.; Liang, W.; Hada, M.; Ehara, M.; Toyota, K.; Fukuda, R.; Hasegawa, J.; Ishida, M.; Nakajima, T.; Honda, Y.; Kitao, O.; Nakai, H.; Vreven, T.; Throssell, K.; Montgomery, J. A., Jr.; Peralta, J. E.; Ogliaro, F.; Bearpark, M. J.; Heyd, J. J.; Brothers, E. N.; Kudin, K. N.; Staroverov, V. N.; Keith, T. A.; Kobayashi, R.; Normand, J.; Raghavachari, K.; Rendell, A. P.; Burant, J. C.; Iyengar, S. S.; Tomasi, J.; Cossi, M.; Millam, J. M.; Klene, M.; Adamo, C.; Cammi, R.; Ochterski, J. W.; Martin, R. L.; Morokuma, K.; Farkas,

O.; Foresman, J. B.; Fox, D. J. Gaussian, Inc., Wallingford CT, 2016.

46. Montgomery JA, Frisch MJ, Ochterski JW, Petersson GA. A complete basis set model chemistry. VI. Use of density functional geometries and frequencies. *J Chem Phys*. 1999;110(6):2822-2827. doi:10.1063/1.477924

47. Xu X, Alecu IM, Truhlar DG. How Well Can Modern Density Functionals Predict Internuclear Distances at Transition States? *J Chem Theory Comput*. 2011;7(6):1667-1676. doi:10.1021/ct2001057

48. Schenker S, Schneider C, Tsogoeva SB, Clark T. Assessment of Popular DFT and Semiempirical Molecular Orbital Techniques for Calculating Relative Transition State Energies and Kinetic Product Distributions in Enantioselective Organocatalytic Reactions. *J Chem Theory Comput*. 2011;7(11):3586-3595. doi:10.1021/ct2002013

49. Simmie JM, Somers KP. Benchmarking Compound Methods (CBS-QB3, CBS-APNO, G3, G4, W1BD) against the Active Thermochemical Tables: A Litmus Test for Cost-Effective Molecular Formation Enthalpies. *J Phys Chem A*. 2015;119(28):7235-7246. doi:10.1021/jp511403a

50. J. B. Burkholder, S. P. Sander, J. Abbatt, J. R. Barker, C. Cappa, J. D. Crounse, T. S. Dibble, R. E. Huie, C. E. Kolb, M. J. Kurylo, V. L. Orkin, C. J. Percival, D. M. Wilmouth, and P. H. Wine "Chemical Kinetics and Photochemical Data for Use in Atmospheric Studies, Evaluation No. 19," JPL Publication 19-5, Jet Propulsion Laboratory, Pasadena, 2019 https://jpldataeval.jpl.nasa.gov.; 2019.

51. Buras ZJ, Elsamra RMI, Green WH. Direct Determination of the Simplest Criegee Intermediate (CH_2OO) Self Reaction Rate. *J Phys Chem Lett*. 2014;5(13):2224-2228. doi:10.1021/jz5008406

52. Chhantyal-Pun R, Davey A, Shallcross DE, Percival CJ, Orr-Ewing AJ. A kinetic study of the CH_2OO Criegee intermediate self-reaction, reaction with SO_2 and unimolecular reaction using cavity ring-down spectroscopy. *Phys Chem Chem Phys*. 2015;17(5):3617-3626. doi:10.1039/C4CP04198D

53. Watson NAI, Black JA, Stonelake TM, Knowles PJ, Beames JM. An Extended Computational Study of Criegee Intermediate–Alcohol Reactions. *J Phys Chem A*. 2019;123(1):218-229. doi:10.1021/acs.jpca.8b09349

54. Aroeira GJR, Abbott AS, Elliott SN, Turney JM, Schaefer HF. The addition of methanol to Criegee intermediates. *Phys Chem Chem Phys*. 2019;21(32):17760-17771. doi:10.1039/C9CP03480C

55. Nakanishi H, Morita H, Nagakura S. Charge-Transfer Character in the Intramolecular Hydrogen Bond: Vacuum Ultraviolet Spectra of Acetylacetone and Its Fluoro Derivatives. *Bull Chem Soc Jpn*. 1978;51(6):1723-1729. doi:10.1246/bcsj.51.1723

56. Belova NV, Oberhammer H, Trang NH, Girichev GV. Tautomeric Properties and Gas-Phase Structure of Acetylacetone. *J Org Chem*. 2014;79(12):5412-5419. doi:10.1021/jo402814c

57. Antonov I, Voronova K, Chen MW, et al. To Boldly Look Where No One Has Looked Before: Identifying the Primary Photoproducts of Acetylacetone. *J Phys Chem A*. 2019;123(26):5472-5490. doi:10.1021/acs.jpca.9b04640

58. McGillen MR, Archibald AT, Carey T, et al. Structure–activity relationship (SAR) for the prediction of gas-phase ozonolysis rate coefficients: an extension towards heteroatomic unsaturated species. *Phys Chem Chem Phys*. 2011;13(7):2842-2849. doi:10.1039/C0CP01732A

59. Klotz B, Graedler F, Sørensen S, Barnes I, Becker KH. A kinetic study of the atmospheric photolysis of α-dicarbonyls. *Int J Chem Kinet*. 2001;33(1):9-20. doi:10.1002/1097-4601(20010101)33:1<9::AID-KIN2>3.0.CO;2-V

60. Messaadia L, El Dib G, Ferhati A, Chakir A. UV–visible spectra and gas-phase rate coefficients for the reaction of 2,3-pentanedione and 2,4-pentanedione with OH radicals. *Chem Phys Lett*. 2015;626:73-79. doi:10.1016/j.cplett.2015.02.032

61. Lee KLK, Nauta K, Kable SH. Photodissociation of acetone from 266 to 312 nm: Dynamics of CH_3 + CH_3CO channels on the S_0 and T_1 states. *J Chem Phys*. 2017;146(4):044304. doi:10.1063/1.4974035

62. Zhou S, Barnes I, Zhu T, Bejan I, Albu M, Benter T. Atmospheric Chemistry of Acetylacetone. *Environ Sci Technol*. 2008;42(21):7905-7910. doi:10.1021/es8010282

63. Atkinson R, Baulch DL, Cox RA, et al. Evaluated kinetic and photochemical data for atmospheric chemistry: Volume II – gas phase reactions of organic species. *Atmos Chem Phys*. 2006;6(11):3625-4055. doi:10.5194/acp-6-3625-2006

64. Dagaut P, Wallington TJ, Liu R, Kurylo MJ. A kinetic investigation of the gas-phase reactions of hydroxyl radicals with cyclic ketones and diones: mechanistic insights. *J Phys Chem*. 1988;92(15):4375-4377. doi:10.1021/j100326a026

65. Novelli A, Hens K, Tatum Ernest C, et al. Estimating the atmospheric concentration of Criegee intermediates and their possible interference in a FAGE-LIF instrument. *Atmos Chem Phys*. 2017;17(12):7807-7826. doi:10.5194/acp-17-7807-2017

66. Finlayson-Pitts BJ, Pitts JN. *Chemistry of the Upper and Lower Atmosphere: Theory, Experiments, and Applications*. Academic Press; 2000.

67. Seinfeld JH, Pandis SN. *Atmospheric Chemistry and Physics: From Air Pollution to Climate Change*. Wiley; 2012.

68. King MD, Canosa-Mas CE, Wayne RP. Frontier molecular orbital correlations for predicting rate constants between alkenes and the tropospheric oxidants NO_3, OH and O_3. *Phys Chem Chem Phys*. 1999;1(9):2231-2238. doi:10.1039/A901192G

69. Pfrang C, King MD, Canosa-Mas CE, Wayne RP. Correlations for gas-phase reactions of NO_3, OH and O_3 with alkenes: An update. *Atmos Environ*. 2006;40(6):1170-1179. doi:10.1016/j.atmosenv.2005.10.019

70. Pfrang C, King MD, Canosa-Mas CE, Wayne RP. Structure–activity relations (SARs) for gas-phase reactions of NO_3, OH and O_3 with alkenes: An update. *Atmos Environ*. 2006;40(6):1180-1186. doi:10.1016/j.atmosenv.2005.09.080

71. McGillen MR, Carey TJ, Archibald AT, Wenger JC, Shallcross DE, Percival CJ. Structure–activity relationship (SAR) for the gas-phase ozonolysis of aliphatic alkenes and dialkenes. *Phys Chem Chem Phys*. 2008;10(13):1757-1768. doi:10.1039/B715394E

72. Jenkin ME, Valorso R, Aumont B, Newland MJ, Rickard AR. Estimation of rate coefficients for the reactions of O_3 with unsaturated organic compounds for use in automated mechanism construction. *Atmos Chem Phys*. 2020;20(21):12921-12937. doi:10.5194/acp-20-12921-2020